Analytical Chemistry Research 12 (2017) 74–81

Contents lists available at ScienceDirect

Analytical Chemistry Research

journal homepage: www.elsevier.com/locate/ancr

Sensors based on Ag-loaded hematite (α-Fe_2O_3) nanoparticles for methyl mercaptan detection at room temperature

Daniel Garcia [a], Gino Picasso [a,*], Pilar Hidalgo [b], Henrique E.M. Peres [c], Rosario Sun Kou [d], Josué M. Gonçalves [e]

[a] Laboratory of Physical Chemistry Research, Faculty of Sciences, National University of Engineering, Av. Tupac Amaru 210, Rimac, Lima 25, Peru
[b] Laboratory of Nanotechnology, Faculty of Gama, Area Especial de Indústria Projeção A, UNB – DF-480, University of Brasilia, Gama Leste, Brasilia DF, 72444-240, Brazil
[c] Department of Electronic System Engineering, EPUSP, University of São Paulo, Av. Prof. Luciano Gualberto, 158, Trav. 3, São Paulo, SP, 05508-900, Brazil
[d] Department of Sciences, Section of Chemistry, Pontifical Catholic University of Peru, Av. Universitaria 1801, San Miguel, Lima 32, Peru
[e] Department of Fundamental Chemistry, Institute of Chemistry, University of São Paulo, Av. Prof. Lineu Prestes 748, Butanta, São Paulo, 05508-000, Brazil

ARTICLE INFO

Article history:
Received 24 October 2016
Received in revised form
11 December 2016
Accepted 12 December 2016
Available online 19 December 2016

Keywords:
Hematite
Gas sensor
Ag-loaded hematite
Methyl mercaptan

ABSTRACT

Sensors based on Ag/α-Fe_2O_3 nanoparticles have been prepared by the coprecipitation method for sensing methyl mercaptan at room temperature. X-ray diffraction patterns of samples matched perfectly with characteristic peaks of hematite with no peaks assigned to Ag even at the highest concentration. STEM images and EDX analysis revealed the presence of Ag nanoparticles (from 2 to 5 nm) which were highly dispersed onto α-Fe_2O_3 surface with an Ag/Fe ratio from 0.014 to 0.099. The Ag nanoparticles were deposited on the hematite surface. Sensing tests of Ag-loaded hematite nanoparticles showed much higher response signal than the unmodified sensor. Hematite loaded with 3%(Wt) Ag showed the highest response with a linear dependence from 20 to 80 ppm. The sensor also depicted a good selectivity and stability during 4 days with short recovery time. The high dispersion of reduced Ag evaluated by XPS analysis played an important chemical role in the sensing mechanism that favored the contact of CH_3SH with oxygen.

1. Introduction

Methyl mercaptan (CH_3SH) is a quite well gas known as a standard additive of some gases as natural gas and propane to facilitate the detection of a gas leak and it is also used in ventilation operation systems to alert mine operators of an emergency. The recommended airborne exposure is 0.5 ppm over an 8-h work shift, not to be exceeded at any time [1]. At higher concentrations, that may be encountered in a laboratory, the gas can cause irritation to the eyes and throat, drowsiness and even bronchitis [2]. The gas can be found in paper and pulp mills and it occurs naturally in some vegetables as onions, garlic, and also in coal tar and petroleum distillates. It is used as an intermediate in the production of pesticides, fungicides, jet fuel and plastics and in the synthesis of methionine as well as a gas deodorant for natural gas, propane and butane [3,4]. The design of an appropriate sensor for rapid measurement of low concentrations of methyl mercaptan demands the development of highly selective sensors with easy manipulation and good reliability.

Different sensing materials have been tested for detection of methyl mercaptan like yttria-stabilized zirconia (YSZ) [5], electronic nose [6], fluorescein mercury (II) acetate (FMA) [7], oxygen sensitive optical fiber [8], among others. Even though these devices present high signal response, the starting material is not accessible and the operating temperature is usually high. As a consequence, previous usage of energy is required and limited.

Metal oxides are the most suitable materials for gas detection due to their irreversible chemical transformations at the surface which allowed them to change their resistance when a testing gas is applied [9]. Particularly, iron oxide as hematite has been used as a sensor in many applications for its semiconductor properties [10–12]. Hematite was applied in different forms: as solid and hollow spindles to sense 2-propanol and acetone [13], as porous α-Fe_2O_3 nanospheres to detect glycine [14], as nanorods via the co-precipitation of $FeCl_3$ with NaOH solutions to detect rhodamine B colorant [15], as an iron oxide thin film grown by atomic layer

* Corresponding author.
E-mail address: gpicasso@uni.edu.pe (G. Picasso).

http://dx.doi.org/10.1016/j.ancr.2016.12.001

deposition to sense O_2 and CO [16], as porous Fe_2O_3 nanostructures to measure H_2S concentrations [17], among others. Hematite has proved to be an interesting material for gas sensing applications, but its use at high working temperatures (normally higher than 25 °C) has restricted its potential applications [16]. The semiconductor properties of hematite in addition to the nanosized distribution of its particles are expected to increase the specific surface area and adsorption activity [18–20]. In order to improve sensitivity and stability for practical applications, hematite is usually loaded with some noble metals such as Au [21], Pd [22,23] and Ag [24], which are claimed to create active sites through electronic and chemical sensitization [25].

Some greenhouse gases such as CO and LPG have been tested with sensors based on α-Fe_2O_3 [16,18,20,23]. In these works, the operating temperatures of the sensor material have been usually higher than 150 °C and the preparation method required long-term treatments and high-cost precursors. The challenge in this paper was to apply a feasible low-cost hematite sensor to detect methyl mercaptan operating at ambient temperatures with high sensitivity and stability, also using Ag which is a cheap noble metal. As far to our knowledge, the application of Ag-modified hematite for the detection of methyl mercaptan is novel and the purpose of this work was to correlate the preparation, structure and texture variables of sensor samples with their response signal and selectivity. To this aim, some sensors based on Ag/α-Fe_2O_3 nanoparticles were prepared for the detection of methyl mercaptan and the role of interaction between the nano-sized hematite and the metal in the sensory properties was explored.

2. Material and methods

2.1. Preparation of Ag/α-Fe_2O_3 nanoparticles

All chemicals used were analytical grade. Ag/α-Fe_2O_3 nanoparticles were prepared by the co-precipitation method from 0.1 mol L^{-1} $Fe(NO_3)_3 \cdot 9H_2O$ (MERCK, 99%) and 0.5 mol L^{-1} $AgNO_3$ (ALDRICH, 99.99%). Mixed solutions of metallic salts (in specific proportions) were added dropwise to an aqueous solution of 0.3 mol L^{-1} Na_2CO_3 (anhydrous, MERCK, 99.9%) with 0.2 wt% polyethylene glycol, used as a surfactant agent, under vigorous stirring at 80 °C [24]. Afterwards, to the prepared metallic solution, an additional quantity of enough sodium carbonate was added to the prepared metallic solution in order to obtain a pH up to 9.8 [25]. The obtained solution was continuously stirred for 2 h and then, it was aged for 12 h at room temperature. Finished the aging time, the precipitate was filtered, washed with deionized water and dried for 1 h at 120 °C. Then, the solid powder was calcined at 400 °C for 1 h at a heating rate of 2 °C per minute [16]. This procedure pursued to stabilize the material sensor in order to prevent changes in the response signal for the operating conditions. In fact, mesoporous α-Fe_2O_3 and samples based on Ag/α-Fe_2O_3 with different amount of Ag (from 1.0 to 5.0 wt%) have been prepared.

2.2. Preparation of alumina supports

All the prepared samples were coated onto an alumina support, Fig. 1a. The support dimensions were adjusted to be used in the experimental setup, designed to test gas sensor materials. Geometric dimensions of supports were 25mm×25mm×2mm (Fig. 1b). On the front side, four interdigital gold electrodes of 0.5 mm of thickness were fixed (Fig. 1b). The geometry of the sensor has been designed to maximize gas-solid contact [26]. The material sensor was dispersed in ethylene glycol to make up an impregnation paste which was applied over the alumina surface by the screen printing technique [27], Fig. 1a. In order to stabilize and attach the active phase onto gold electrodes, the sensor was slowly heated at 2 °C/min and held at 400 °C for 8 h, allowing complete solvent evaporation.

2.3. Experimental set-up to test sensors

Sensors have been tested in the experimental set-up showed in Fig. S1. The system consists of 3 sections:

(a) A feed section containing two mass flow controllers, one for standard methylmercaptan (LINDE 1% in N_2) and the other one for compressed dry air (<5 ppm of H_2O), LINDE 99% used as a dilution gas to obtain working concentrations ranging from 20 to 80 ppm.
(b) An analysis section equivalent to a gas chamber with hermetic lock where alumina-deposited sensor was assembled over Ni–Cr resistance and connected online with a Semiconductor Device Parameter Analyzer Agilent B1500A to measure the electrical resistance. The chamber has a duct at the entrance and at the exit through producing gas feed transportation in and out of the system. The gas composition at the exit of the gas chamber was evaluated by an on-line gas chromatograph (VARIAN 450-GC) provided with TCD and FID detector.
(c) A recorder section for the acquisition and analysis of data using the software Start Easy Expert (Fig. S1).

In the experimental essays, one of the pair of the electrodes has been used as a reference material. In order to clean all the environmental interferences placed over the sensor surface and inside the analysis camera, the electrode surfaces of sensors were previously washed using nitrogen with a flux of 100 cc/min for 2 h. Some previous electrical tests were made applying a voltage work scale from 0 to 10 V with a step of 0.1 V and applying a current frontier of 100 mA to verify the linear dependence of output signal I as a function of V.

Each electrical response of sensors was calculated as the ratio % $\Delta R/R_{air}$, where ΔR is the difference between response signal measured in the presence of gas (R_{gas}) and air (R_{air}). After each experimental acquirement, a flux of nitrogen was passed through the system to clean the surface.

The samples were characterized by the following techniques:

1. Thermogravimetric and Differential Scanning Calorimetry (TG-DSC) analysis were performed using a TA Instrument SDT Q600 to study the thermal treatments of sample preparation. Therefore, Ag-loaded hematite samples were analyzed in a nitrogen atmosphere for temperatures from 25 °C up to 600 °C, with a heating rate of 10 °C/min.
2. XRD analysis was performed to study the crystallographic structure of the material. Analyses were made using a diffractometer RIGAKU (Miniflex600) operating with the following parameters: Cu Kα radiation (λ = 1.5418 Å), 15 mA, 30 kV, Ni filter, 2θ scanning range 4–70°, and scan step size of 0.04° per second. The crystal phases were identified using PDF2 database from International Centre for Diffraction Data (ICDD). The mean crystallite sizes were estimated from the Scherrer equation and the selected reflection peaks were fitted by a Gaussian function.
3. The textural properties of solids were studied by N_2-sorption measurements at liquid nitrogen temperature using a Micromeritics GEMINI VII-2390t instrument. Prior to the adsorption experiments, the samples were degassed under vacuum by helium at 250 °C for 3 h. The specific surface area was calculated according to the BET method. Also, the pore size distribution and the mean pore size were evaluated using the BJH (Barrett-

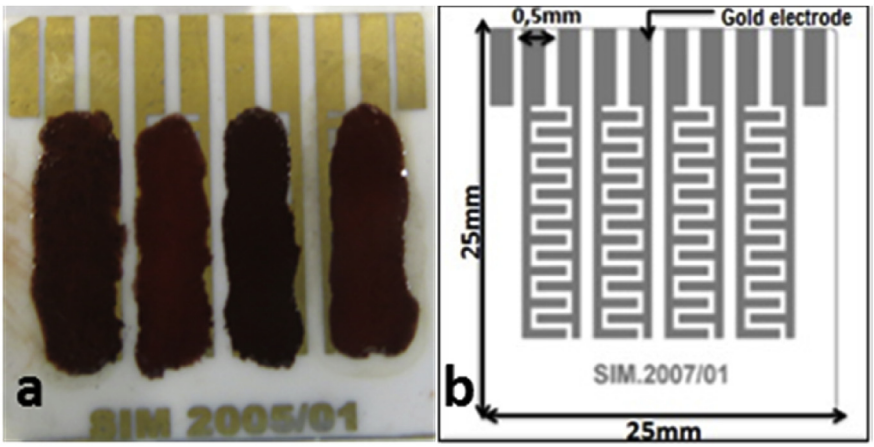

Fig. 1. (a) Alumina substrate after deposition of four samples, (b) design of applied substrate containing gold electrodes.

Joyner-Halenda) procedure, applied to the desorption branch of the isotherm.

4. X-ray photoelectron spectra (XPS) of the fresh and used sensors were acquired to test the surface redox chemistry of metal ions. Analysis were made using a VG Escalab 200R spectrometer equipped with a hemispherical electron analyzer and an X-ray source of Al Kα1 ($h\nu = 1486.6$ eV, 1 eV = 1.6302×10^{-19} J) 120 W. The powder samples were placed in a pretreatment chamber and degassed at 573 K. All binding energies (BE) were referred to the C1s peak used as an internal standard (284.9 eV).
5. Energy dispersive X-ray fluorescence measurements, EDXRF, were carried out using an EDX720 instrument from Shimadzu, equipped with a X-ray tube with a Rh target and a Si(Li) detector, working at 5–15 kV.
6. Transmission Electron Microscopy (TEM) images or Scanning Transmission Electron Microscopy (STEM) image mode were obtained in a JEOL JEM-2100 FEG equipment at an accelerating voltage of 200 kV. Samples were prepared by dispersing them with 3 μL of suspension in acetone over an ultrathin carbon film on the 400 mesh copper grids (TedPella).
7. Scanning electron microscopy with energy dispersive spectroscopy was performed in a FEG-SEM JEOL JSM – 4701F equipment. The data were collected with accelerating voltage of 20.0 kV and magnification equal to ×430. The recorded transitions in spot 1 were Fe–K and Ag-L.
8. Iron and silver composition were analyzed with a SPECTRO ARCOS ICP-OES analyzer. The modified samples were dissolved in a mixture of 4 mL of aqua regia and Milli Q water until reaching a volume up to 50 mL. The operating conditions were adjusted to maximize the output signal.

3. Results and discussion

3.1. Thermogravimetric analysis and differential scanning calorimetry (TGA-DSC)

TGA and DSC analysis of the uncalcined hematite sample modified with 3 wt% Ag has been simultaneously performed in order to study the temperature effect on the stability of sensor, i.e. after precipitation and drying treatment. From DSC analysis as is shown in Fig. 2, a drastic loss of weight was observed with the formation of an endothermic peak at around 100 °C, which could be attributed to the dehydration of the sample. In the range from 200 to 400 °C, the exothermic peak may be assigned to the residual nitrate ions from precursor and the transformation reaction of

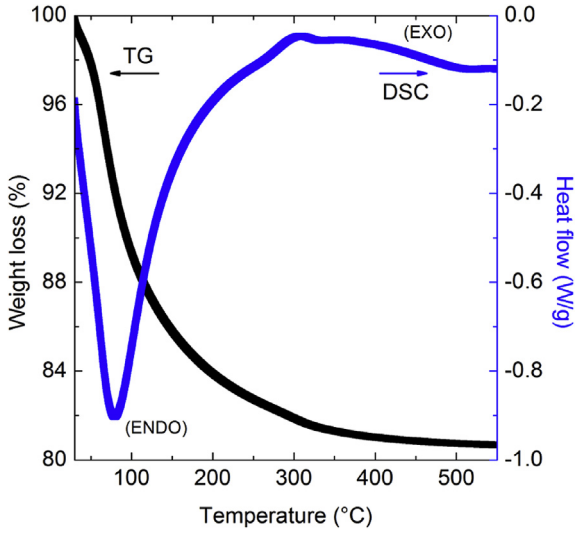

Fig. 2. TGA and DSC of 3 wt% Ag/FeOOH.

FeOOH to Fe_2O_3. Additionally, TGA shows that above 400 °C there is no significant loss of mass, indicating that the temperature of 400 °C is the suitable calcination temperature under air atmosphere; it agrees with the results previously reported [23]. The presence of water and hematite – goethite phases was confirmed in previous work [16]. As a consequence, the loss of weight observed in Fig. 2 could be attributed to the reaction (1):

$$2(2Fe_2O_3 \cdot FeOOH \cdot 4H_2O) \rightarrow 5Fe_2O_3 + 9H_2O \quad (1)$$

For starting mass of 28.2 mg, the final mass loss obtained was about 4.8 mg, which is 82.3%, very near to the theoretical value 80.9%, confirming a phase transformation to hematite.

3.2. X-ray diffraction (XRD) and textural surface analysis

The diffraction patterns of all prepared sensors based on α-Fe_2O_3 matched perfectly with the characteristic peaks of the standard hematite reflections (JCPDS – International Centre for Diffraction Data N° 33-0664) as is shown in Fig. 3. No peaks were assigned to Ag. When additive ions are introduced into a powder, they may: (a) diffuse into the bulk of the particle; (b) migrate to the surface; or

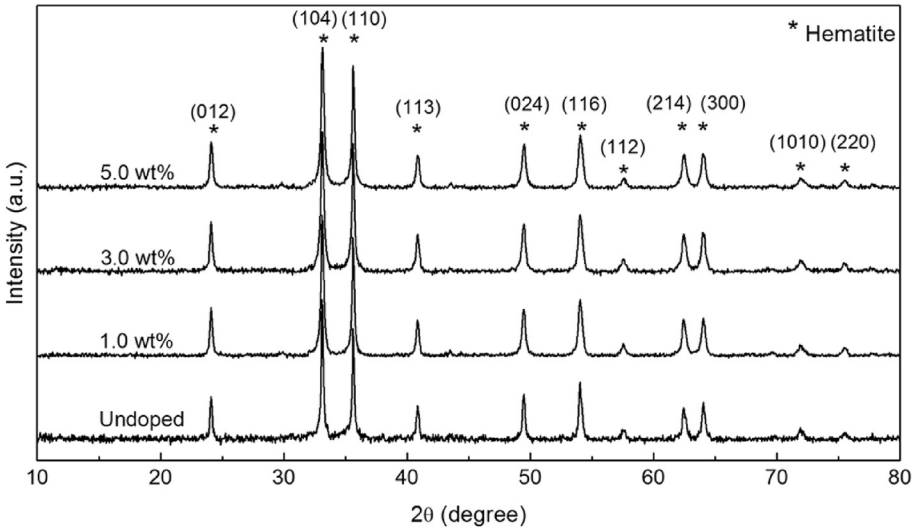

Fig. 3. XRD patterns of prepared samples based on Ag/α-Fe_2O_3 nanoparticles.

even (c) nucleate a new phase. Since the ionic radius of Ag^+ (1.15 Å) is much higher than that corresponding to Fe^{3+} (0.635 Å), it is therefore reasonable to consider the migration of Ag particles on the surface of α-Fe_2O_3 [24]. Furthermore, the crystallite mean size of all samples was calculated applying Scherrer equation from the main peaks and the results are shown in Table 1. Regarding the textural properties, all the N_2-sorption isotherms of the samples corresponded to type IV, typical to micro-mesoporous materials as is displayed in Fig. 4, for the sample 3 wt% Ag, which is shown as a representative sample. The hysteresis loop of type H1 revealed the presence of cylindrical pores. Also, the average pore size, evaluated by BJH method, was around 8–10 nm, which reveals the normal size distribution typical to these surfaces (Fig. 4). Additionally, as is observed in Table 1, all prepared materials keep strong linear correlation between crystallite size and specific surface area. The decreasing of BET surface of sample 5 wt% Ag related to the 3 wt% Ag modified sample is probably caused by the inhibition of segregation as a consequence of sinterization of particles.

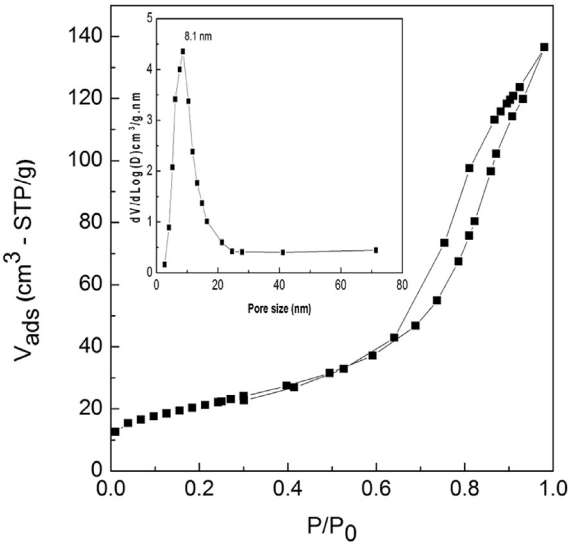

Fig. 4. BET Isotherm of 3 wt% Ag sample.

3.3. X-ray photoelectron spectroscopy (XPS)

XPS was used to analyze the elemental composition on the surface into 10 nm depth. In Fig. 5a, the XPS spectra revealed that peaks of Fe $2p_{3/2}$ and Fe $2p_{1/2}$ match with the binding energies of 711.0 ± 0.2eV and 724.5 ± 0.2eV, respectively, indicating the presence of Fe^{3+} species at the outer layer of the surface which is supported by the literature values [28]. Fig. 5b shows well-defined peaks of the Ag3d doublets for sample 3 wt% Ag with the binding energies of 368.2 ± 0.1eV and 374.1 ± 0.1eV which correspond to Ag $3d_{5/2}$ and Ag $3d_{3/2}$, respectively; therefore, the probable state of Ag in the composite sample is metallic on the surface, as it was shown in previous works [24,29]. The elemental surface composition of the ratio Ag/Fe over the surface of α-Fe_2O_3 is much higher than its bulk counterpart (Table 2), indicating that Ag is quite well dispersed. The well-defined peaks are probably due to electrons that have not lost energy in emerging from the sample [30].

Table 1
Specific surface area (BET) and crystallite size (Scherrer) of all synthesized samples.

Sample (wt% Ag)	Crystallite size (nm)	S_{BET} (g/m^2)
Unmodified	39.3	41
1.0	31.2	57
3.0	27.5	74
5.0	28.6	60

3.4. Scanning transmission electron microscopy (STEM)

The STEM images of sample 3 wt% Ag display that Ag nanoparticles (dark) grew on α-Fe_2O_3 surface (bright) as is shown in Fig. 6a. The collected STEM bright-field and dark-field images just reveal the presence of two elements with low and high atomic number, but considering the EDX analysis (Table 3), these two elements corresponds to Fe and Ag, respectively. Fig. 6b shows the same image in STEM dark field mode, where the diffracted electrons collected from Ag particles are bright. By the way, this dual image is based on the process of scattering of electrons caused by heavier Ag atoms in comparison to Fe. Moreover, Fig. 6c and d were recorded using higher magnification and it allows to see closely the silver nanoparticles on the hematite surface. According to Fig. 6e, the particle size is around 40–50 nm. The TEM micrographs and the

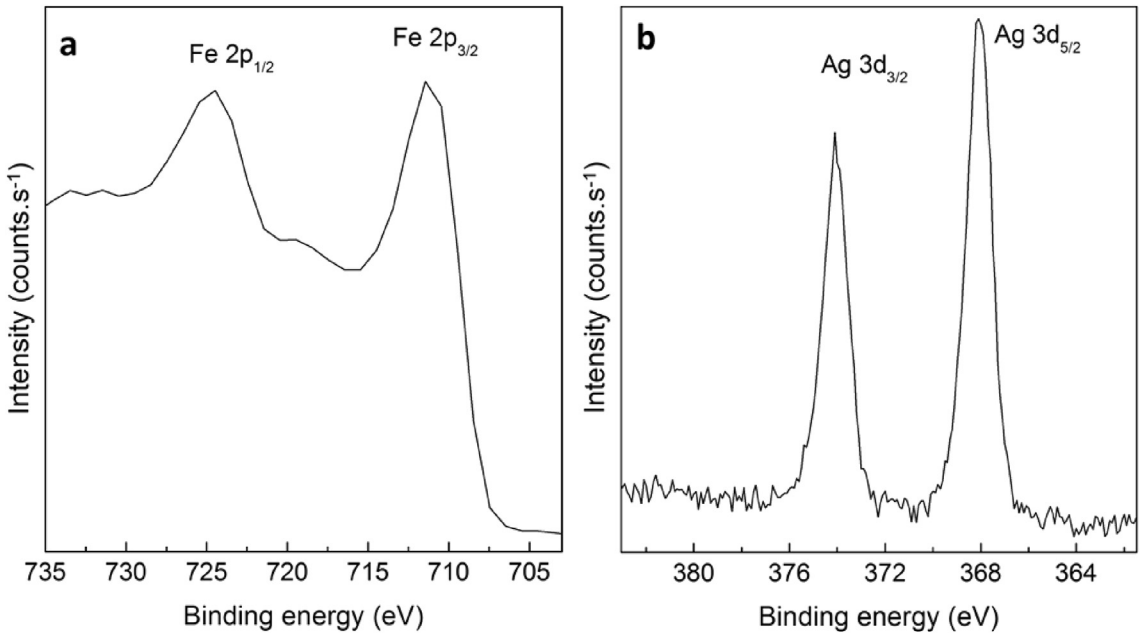

Fig. 5. XPS spectra of sample 3 wt% Ag, corresponding to (a) Fe 2p and (b) Ag 3d.

Table 2
Elemental composition and binding energies of Fe $2p_{3/2}$ and Ag $3d_{5/2}$, corresponding to Ag-modified samples.

Sample (wt% Ag)	Ag/Fe (XPS)	Ag/Fe (bulk)	Binding energy (eV) (% atom.)	
			Fe $2p_{3/2}$	Ag $3d_{5/2}$
Unmodified	–	–	710.8 (28.69%)	–
1.0%	1/12	1/70	710.7 (30.57%)	368.1 (2.5%)
3.0%	1/5	1/14	711.0 19.01%	368.2 (4.2%)

sustained enrichment of Ag in the samples due to the higher experimental ratios of Ag/Fe than nominal value (Table 3) reinforce the idea that Ag nanoparticles (2–5 nm) are anchoring to the hematite surface. From the HRTEM image of sample 3 wt% Ag (Fig. 6f), the fringe spacing of 0.23 nm corresponds to ⟨111⟩ planes of silver, while the other distance (for d = 0.27 nm) is agreed with the successive ⟨104⟩ planes of hematite.

3.5. ICP analysis

The ICP analysis revealed that the mass ratio of Ag/Fe of each sample is close to the theoretical values (Table S1). Moreover, the SEM/EDS analysis of 3 wt% Ag showed in situ the dispersion of Ag nanoparticles on hematite (Fig. S2). According to the ICP approach, the corresponding percentages for Ag nominal loadings of 1.0%, 3.0% and 5.0% are 0.9%, 2.7% and 5.5%, respectively. These values are relatively near to their nominal counterparts. Even more, from the EDS analysis on SEM spot 1 it could be inferred that the Ag nanoparticles (for Ag/Fe = 0.04210) are found homogenously dispersed on hematite and this value match perfectly with ICP-OES analysis.

3.6. Gas sensing characterization

The gas response of the gas sensors has been evaluated by the relative variation of the electrical resistance, as follows:

$$\%\left(\frac{\Delta R}{R_{air}}\right) = \frac{R_{gas} - R_{air}}{R_{air}} \times 100\%$$

where, R_{gas} and R_{air} are the electrical resistances of the sample under atmosphere of CH_3SH and air, respectively. Prior to the experiments, the linear behavior of the voltage as a function of current intensity was verified. The sample tests for detection of methyl mercaptan were made setting initial concentration of 80 ppm at room temperature (Fig. 7). As a result, the Ag-modified samples showed higher responses than the unmodified sample, implying sensitivity enhancement caused by the presence of Ag in the samples. Indeed, the 3 wt% Ag had the highest surface area, so electrical response should also depend upon surface area. In fact, the results reveal that the gas response strongly depends on the surface area and Ag content which is usually sensitive to thiol groups [31,32]. The surface metallic state of Ag, depicted from XPS analysis, played an additional promoting role via chemical sensitization, which is common when the active phase is in reduced state [33,34]. Therefore, Ag as a catalyst enhanced the adsorption of the substrate, improving the electron exchange between the sensor and the testing gas [34]. For the sample 3 wt% Ag, Fig. 8a depicts the maximum of the resistance variation for each tested concentration. From this plot, one can verify a very linear response of the sensors (Fig. 8b). The gas responses of all sensors showed a direct dependence in relation to the concentrations in the range from 20 to 80 ppm at room temperature, with a very good reproducibility, as is illustrated in Fig. 8a, for sample 3 wt% Ag.

The response or recovery time is an important factor of sensor performance describing the time in which the measured signal reaches 90% of maximum of gas response, after applying or switching off the testing gas, respectively (Fig. 8a) [9]. The recovery times and gas responses are shown in Table 4. The recovery and response times rose up with the concentration of substrate as is expected.

The selectivity of detection is very important for large scale applications. It was selected the sample 3 wt% Ag and three different gases: methane, propane and n-hexane (Fig. 9a). The gas response to methane and propane is almost zero, meanwhile for the n-hexane the gas response is 9%, which is much lower than the response for 80 ppm of methyl mercaptan (72%). In this regard, the gas response of 3 wt% Ag modified sensor showed a good

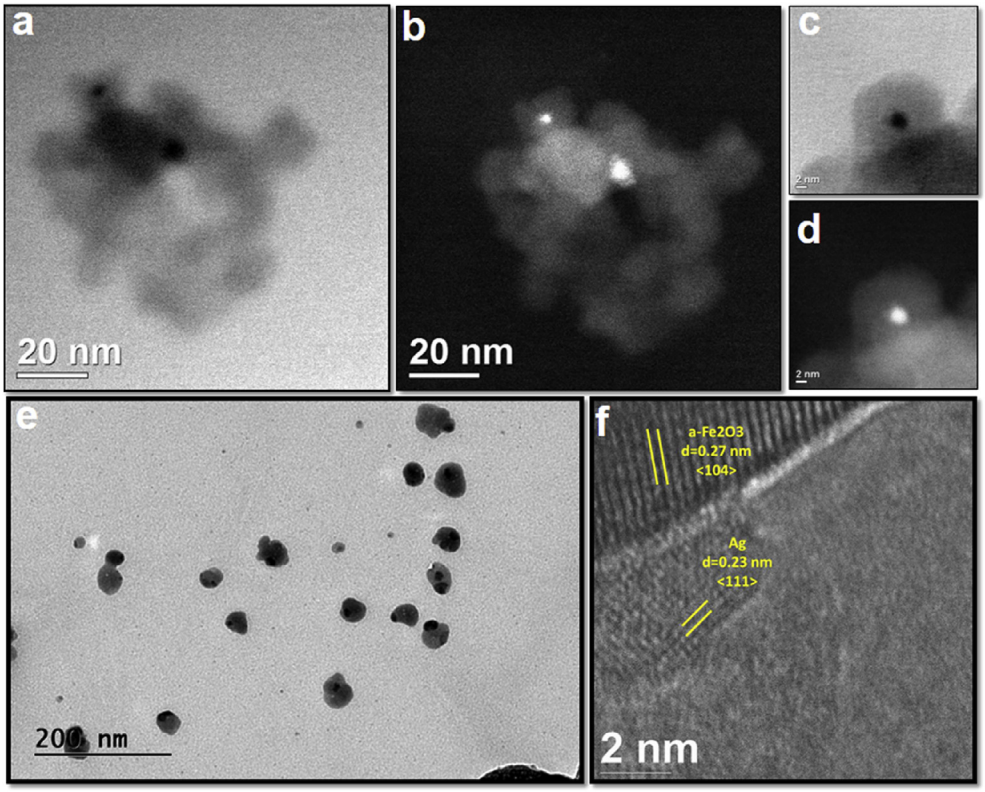

Fig. 6. a,b,c,d: STEM images, e: TEM image, f: HRTEM of sample 3 wt% Ag.

Table 3
EDX values of unmodified and Ag-loaded samples.

Sample (wt% Ag)	Fe (%)[e]	Ag (%)[e]	Ag/Fe[e]
Unmodified	98	0	
1.0	97.39	1.78	0.018
3.0	94.42	4.71	0.049
5.0	90.34	8.96	0.099

e: experimental value.

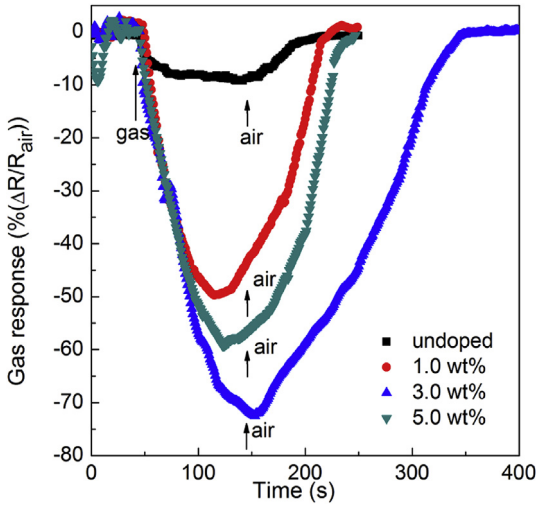

Fig. 7. Gas response of unmodified hematite and Ag modified sensors for 80 ppm of methyl mercaptan.

selectivity, with a much higher significant response signal than the other gases and it could be applied in practical mine operations. In addition, sample 3 wt% Ag showed a good-short term stability during 4 days (Fig. 9b) (see Fig. 10).

3.7. Sensing mechanism

The gas response of n-type semiconductors such as hematite involves electron depletion layer formation and the return of these electrons to the conduction band. Initially, the oxygen molecules from the air pass through the hematite surface and they are adsorbed on the surface according to the reaction (2):

$$O_{2(gas)} \rightarrow O_{2(ads)} \quad (2)$$

Then, the oxygen-free electrons interaction forms oxygen ions with trapped electrons on the hematite surface, as is shown in reaction (3) which is appropriate for temperatures lower than 100 °C [31,32]:

$$O_{2(ads)} + e^- \rightarrow O^-_{2(ads)} \quad (3)$$

As a consequence, an electron depletion layer is formed and this defines the baseline of the hematite. When the methyl mercaptan is delivered to the system, the gas is chemisorbed on the hematite. After that, the methyl mercaptan with previously adsorbed oxygens can be interact via an oxidation reaction and the trapped electrons on the surface are released back to the conduction band producing a decrease of the electrical resistance of hematite, reaction (4):

$$CH_3SH + 3O^-_{2\ (ads)} \rightarrow CO_2 + SO_2 + 2H_2O + 3e^- \quad (4)$$

The addition of small quantities of Ag improves considerably the signal response in regards to the deeper electron depletion layer.

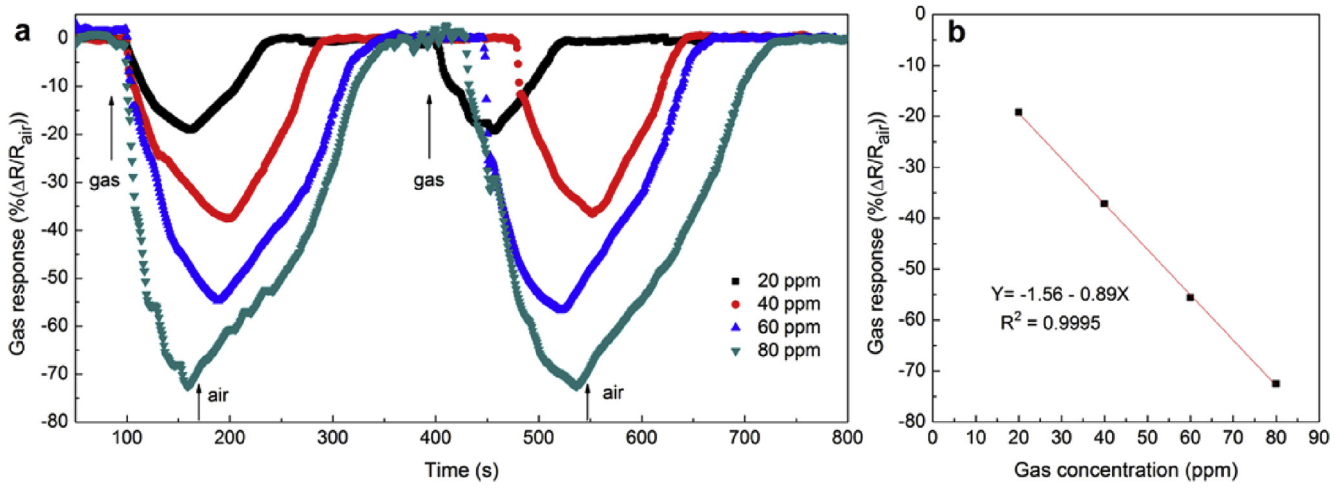

Fig. 8. a: Reproducibility of gas sensing performance of sample 3 wt% Ag for different concentrations of methyl mercaptan, b: linear gas response of the sample 3 wt% Ag as a function of initial concentration of methyl mercaptan.

Table 4
Recovery and response time of the sample 3 wt% Ag with different initial concentrations of methyl mercaptan in the range of 20–80 ppm.

Concentration (ppm)	Response time/Recovery time (s)
20	57/71
40	85/83
60	79/115
80	96/172

The silver on the surface plays the role of catalyst, accelerating the conversion rate of oxygen to ionic oxygen. Consequently, there are higher quantities of trapped electrons that produce a thicker depletion layer. This phenomenon is also promoted with the high surface area of the 3 wt% Ag modified sample (Table 2). When the silver-modified hematite is exposed to methyl mercaptan, these molecules are preferentially chemisorbed because the high affinity of thiol groups for metallic Ag. Indeed, silver accelerates the reaction of methyl mercaptan with oxygen ions via a spillover effect [35] The deep electron depletion layer changes into a flat layer, so this effect and the reduced resistance make that the gas response of Ag/α-Fe_2O_3 becomes greater than the unmodified hematite. The well dispersion of silver nanoparticles as it was shown in 3 wt% Ag by STEM, EDS analysis, enhances the spillover effect.

When the weight percentage of Ag is higher than 3%, the sensor could show an antagonistic effect. The high concentration of silver nanoparticles dispersed on the hematite could create connections among them. Then, this material is going to contain microcircuits of silver on the surface as well as in the body of the 5 wt% Ag-modified sample [35]. This produces that the conduction of electrons happens through the silver, which exhibits better conductivity than the hematite; as a result, the electrical resistance of the material decreases. Therefore, the adsorption of oxygen and the analyte-oxygen interaction decreases considerably. As a consequence, the

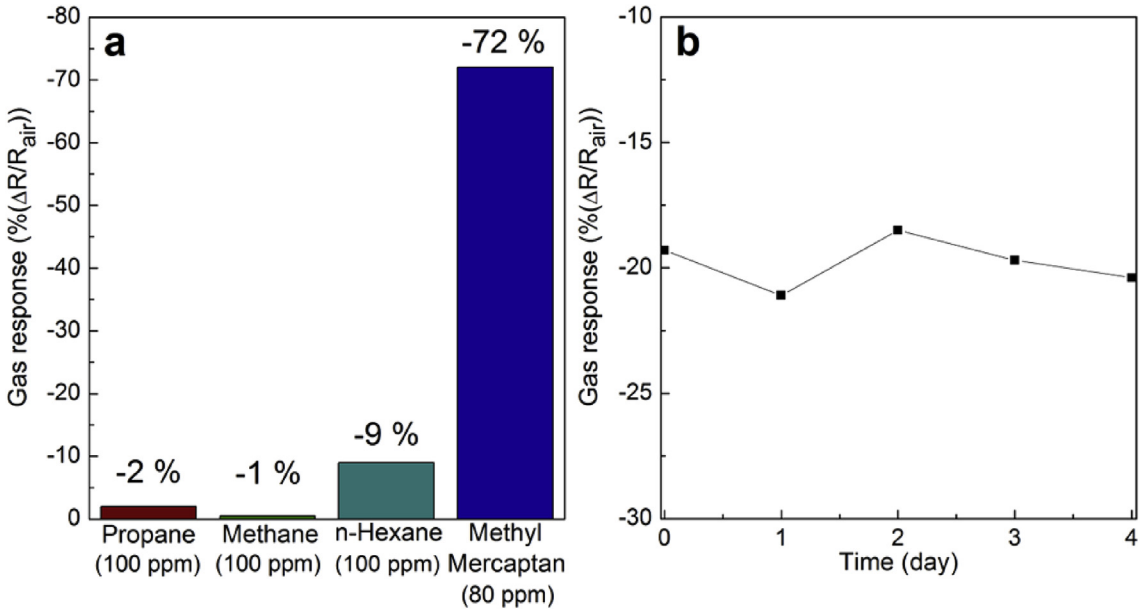

Fig. 9. (a) Selectivity of the sensor 3 wt% Ag/α-Fe_2O_3 to methyl mercaptan at room temperature. (b) Short-term stability of the sensor 3 wt% Ag/α-Fe_2O_3 for 20 ppm of methyl mercaptan at room temperature.

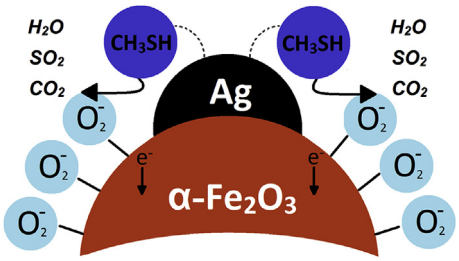

Fig. 10. Chemical influence of Ag nanoparticles on the sensing mechanism.

gas response of 5 wt% Ag is expected to be lower than the 3 wt% Ag-modified hematite.

4. Conclusions

Mesoporous sensors based on nanoparticles of Ag/α-Fe_2O_3 with different metal content (from 1.0 to 5.0 wt% Ag) have been synthesized by the coprecipitation method. A high rate of dispersion of Ag nanoparticles on the surface improved the activity of the sensors. According to the resistance measurements, Ag-modified samples provided much higher resistance variation for detection of CH_3SH than the unmodified hematite at room temperature. The testing of 3 wt% Ag sensor at room temperature in the range of 20–80 ppm for CH_3SH revealed a good linear dependence, which is proportional to the concentration of the testing gas. Therefore, a successful repeatability, a good selectivity and a short-term stability drive this gas sensor to be applied for environmental analysis and industrial process control.

Acknowledgements

The authors gratefully acknowledge the financial support for this work provided by National University of Engineering-Faculty of Sciences and the Institute of Research of National University of Engineering (IGI). The authors are also grateful to Brazilian Nanotechnology National Laboratory – LNNano/CNPEM (Campinas, Brazil) by the STEM facilities. GP acknowledges Dr. Silvia Irusta from the University of Zaragoza (Spain) by the XPS measurements and XRD Laboratory of the National University of San Marcos (Peru) by the XRD facilities.

Appendix A. Supplementary data

Supplementary data related to this article can be found at http://dx.doi.org/10.1016/j.ancr.2016.12.001.

References

[1] http://www.atsdr.cdc.gov/MHMI/mmg139.pdf, accessed on 16 January 2016.
[2] http://www.telegraph.co.uk/news/uknews/9818947/What-is-methyl-mercaptan-gas.html, accessed on 16 January 2016.
[3] http://www.kumed.com/~/media/Imported/kumed/documents/kdhe-20methyl-20mercaptan.ashx, accessed on 16 January 2016.
[4] S. Deshmukh, A. Jana, N. Bhattacharyya, R. Bandyopadhyay, R.A. Pandey, Quantitative determination of pulp and paper industry emissions and associated odor intensity in methyl mercaptan equivalent using electronic nose, Atmos. Environ. 82 (2014) 401–409.
[5] M. Mori, Y. Itagaki, Y. Sadaoka, S. Nakagawa, M. Kida, T. Kojima, Detection of offensive odorant in air with a planar-type potentiometric gas sensor based on YSZ with Au and Pt electrodes, Sens. Actuators B 191 (2014) 351–355.
[6] S. Deshmukh, K. Kamde, A. Jana, S. Korde, R. Bandyopadhyay, R. Sankar, N. Bhattacharyya, R.A. Pandey, Calibration transfer between electronic nose systems for rapid in situ measurement of pulp and paper industry emissions, Anal. Chim. Acta 841 (2014) 58–67.
[7] S. Jayaraman, R. Walia, N. Alagirisamy, Fluorescein mercuric acetate—a novel sensor for oral malodour detection, Sens. Actuators B 148 (2010) 54–58.
[8] K. Mitsubayashi, T. Minamide, K. Otsuka, H. Kudo, H. Saito, Optical bio-sniffer for methyl mercaptan in halitosis, Anal. Chim. Acta 573–574 (2006) 75–80.
[9] M.E. Franke, T.J. Koplin, U. Simon, Metal and metal oxide nanoparticles in chemiresistors: does the nanoscale matter? Small 2 (2006) 36–50.
[10] F.S. Freyria, G. Barrera, P. Tiberto, E. Belluso, D. Levy, G. Saracco, P. Allia, E. Garrone, B. Bonelli, Eu-doped α-Fe_2O_3 nanoparticles with modified magnetic properties, J. Solid State Chem. 201 (2013) 302–311.
[11] H. Ni, Y. Ni, Y. Zhou, J. Hong, Microwave hydrothermal synthesis, characterization and properties of rice-like α-Fe_2O_3 nanorods, Mater. Lett. 73 (2012) 206–208.
[12] W. Zhu, X. Cui, L. Wang, T. Liu, Q. Zhang, Monodisperse porous pod-like hematite: hydrothermal formation, optical absorbance, and magnetic properties, Mater. Lett. 65 (2011) 1003–1006.
[13] J. Huang, M. Yang, C. Gu, M. Zhai, Y. Sun, J. Liu, Hematite solid and hollow spindles: selective synthesis and application in gas sensor and photocatalysis, Mater. Res. Bull. 46 (2011) 1211–1218.
[14] H. Chen, Y. Zhao, M. Yang, J. He, P.K. Chu, J. Zhang, S. Wu, Glycine-assisted hydrothermal synthesis of peculiar porous α-Fe_2O_3 nanospheres with excellent gas-sensing properties, Anal. Chim. Acta 659 (2010) 266–273.
[15] X. Cui, T. Liu, Z. Zhang, L. Wang, S. Zuo, W. Zhu, Hematite nanorods with tunable porous structure: facile hydrothermal-calcination route synthesis, optical and photocatalytic properties, Powder Technol. 266 (2014) 113–119.
[16] M. Aronniemi, J. Saino, J. Lahtinen, Characterization and gas-sensing behavior of an iron oxide thin film prepared by atomic layer deposition, Thin Solid Films 516 (2008) 6110–6115.
[17] Q. Hao, L. Li, X. Yin, S. Liu, Q. Li, T. Wang, Anomalous conductivity-type transition sensing behaviors of n-type porous -Fe_2O_3 nanostructures toward H_2S, Mater. Sci. Eng. B 176 (2011) 600–605.
[18] V.V. Jadhava, S.A. Patil, D.V. Shinde, S.D. Waghmare, M.K. Zate, R.S. Mane, S.H. Han, Hematite nanostructures: morphology-mediated liquefied petroleum gas sensors, Sens. Actuators B 188 (2013) 669–674.
[19] M.Y. Wang, T. Shen, M. Wang, D.E. Zhang, Z.W. Tong, J. Chen, One-pot synthesis of α-Fe_2O_3 nanoparticles-decorated reduced graphene oxide for efficient nonenzymatic H_2O_2 biosensor, Sens. Actuators B 190 (2014) 645–650.
[20] N.D. Cuong, T.T. Hoa, D.Q. Khieu, N.D. Hoa, N.V. Hieu, Gas sensor based on nanoporous hematite nanoparticles: effect of synthesis pathways on morphology and gas sensing properties, Curr. Appl. Phys. 12 (2012) 1355–1360.
[21] N. Funazaki, A. Hemmi, S. Ito, Y. Asano, S. Yamashita, T. Kobayashi, M. Haruta, Development of carbon monoxide detector using Au fine particles-doped α-Fe_2O_3, Sens. Actuators B 14 (1993) 536–538.
[22] X.C. Jiang, A.B. Yu, Synthesis of Pd/α-Fe_2O_3 nanocomposites for catalytic CO oxidation, J. Mater. Process. Technol. 209 (2009) 4558–4562.
[23] G. Picasso, M.R. Sun Kou, O. Vargasmachuca, J. Rojas, C. Zavala, A. Lopez, S. Irusta, Sensors based on porous Pd-doped hematite (α-Fe_2O_3) for LPG detection, Microporous Mesoporous Mater. 185 (2014) 79–85.
[24] Y. Wang, Y. Wang, J. Cao, F. Kong, H. Xia, J. Zhang, B. Zhu, S. Wang, S. Wu, Low-temperature H_2S sensors based on Ag-doped, α-Fe_2O_3 nanoparticles, Sens. Actuators B 131 (2008) 183–189.
[25] N. Yamazoe, New approaches for improving semiconductor gas sensors, Sens. Actuators B 5 (1991) 7–19.
[26] M. Soresca, L. Diamandescu, A. Tomescu, S. Krupa, Synthesis and sensing properties of zirconium-doped hematite nanoparticles, Phys. B 404 (2009) 2159–2165.
[27] P. Kuberský, T. Syrový, A. Hamácek, S. Nespurek, L. Syrová, Towards a fully printed electrochemical NO_2 sensor on a flexible substrate using ionic liquid based polymer electrolyte, Sens. Actuators B 209 (2015) 1084–1090.
[28] C.D. Wagner, W.M. Riggs, L.E. Davis, J.F. Moulder, Handbook of X-ray photoelectron spectroscopy, 1979, p. 192.
[29] T. Potlog, D. Duca, M. Dobromir, Temperature-dependent growth and XPS of Ag-doped ZnTe thin films deposited by close space sublimation method, Appl. Surf. Sci. 352 (2015) 33–37.
[30] A.M. Ferraria, A.P. Carapeto, A.M. Botelho Do Rego, X-ray photoelectron spectroscopy: silver salts revisited, Vacuum 86 (2012) 1988–1991.
[31] Y. Huang, W. Chen, S. Zhang, Z. Kuang, D. Ao, N. Rafat Alkurd, W. Zhou, W. Liu, W. Shen, Z. Li, A high performance hydrogen sulfide gas sensor based on porous α-Fe_2O_3 operates at room-temperature, Appl. Surf. Sci. 351 (2015) 1025–1033.
[32] B. Huayhuas, J.C.M. Gomero, Maria D.P.T. Sotomayor, Nanostructured screen-printed electrodes modified with self-assembled monolayers for determination of metronidazole in different matrices, J. Braz. Chem. Soc. 25 (2014) 1737–1745.
[33] V.K. Tomer, S. Devi, R. Malik, S.P. Nehra, S. Duhan, Fast response with high performance humidity sensing of Ag–SnO_2/SBA-15 nanohybrid sensors, Microporous Mesoporous Mater. 219 (2016) 240–248.
[34] V.K. Tomer, S. Duhan, A facile nanocasting synthesis of mesoporous Ag-doped SnO_2 nanostructures with enhanced humidity sensing performance, Sens. Actuators B 223 (2016) 750–760.
[35] J. Ding, J. Zhu, P. Yao, J. Li, H. Bi, X. Wang, Synthesis of ZnO–Ag hybrids and their gas-sensing performance toward ethanol, Ind. Eng. Chem. Res. 54 (2015) 8947–8953.